



Wear properties of stir cast and hot extruded Mg-6Zn-1Ca/Al₂O₃p composites

Hassan Jafari¹ · Alireza Mazlounian² · Mohammad Meghdad Fallah³

Received: 20 March 2021 / Accepted: 14 July 2021 / Published online: 30 July 2021
© The Author(s), under exclusive licence to Springer-Verlag GmbH, DE part of Springer Nature 2021

Abstract

Magnesium alloys and composites, because of their notable properties, are currently being investigated to open out wide-spread applications for different industries. In this study, Mg-6Zn-1Ca alloy matrix composite, with different volume percentages of Al₂O₃ reinforcing particles, was produced by stir casting followed by hot extrusion. The microstructure of the cast and extruded alloys and composites was characterized using optical and scanning electron microscopes, energy-dispersive X-ray and X-ray diffraction spectroscopies. All produced samples were then undergone hardness and wear experiments. Microstructural observations indicated that Ca₂Mg₆Zn₃ precipitates are often located at the grain boundaries of the α-Mg matrix. The observations also showed that increasing the amount of Al₂O₃ not only increases the hardness but also improves the wear resistance of both the cast and extruded samples, although wear resistance of the extruded composites was much higher than that of the cast samples. Besides, increasing the extrusion temperature from 350 °C to 400 °C increased the wear rate, and the composites extruded at 350 °C possessed the best wear resistance among samples. The results also showed that a combination of the abrasive, delamination and adhesive wear mechanisms takes place in composites, although abrasion is the predominant mechanism in the composites extruded at 350 °C.

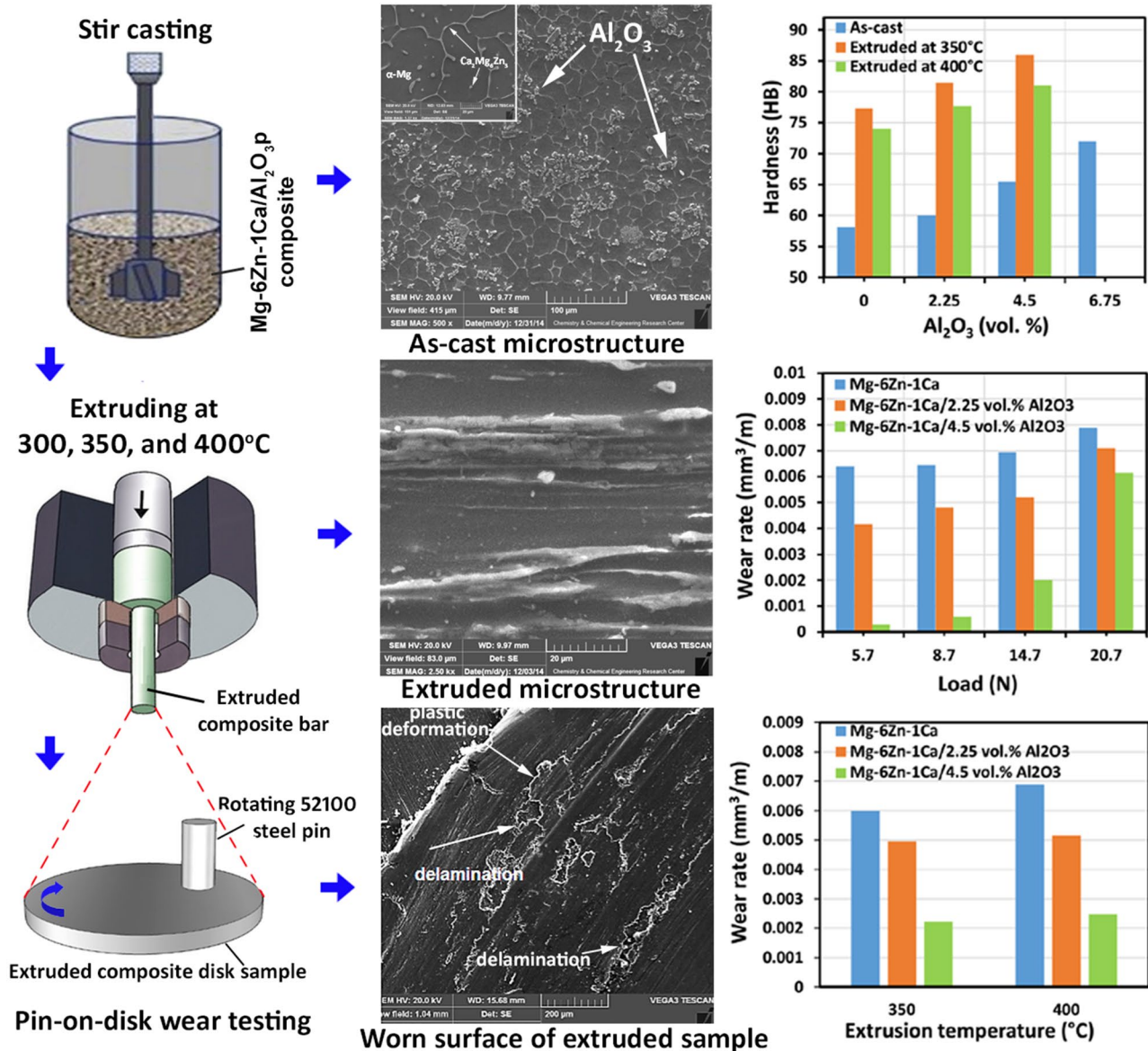
✉ Hassan Jafari
jafari_h@yahoo.com; hjafari@sru.ac.ir

¹ Materials Engineering Department, Faculty of Materials Engineering and Interdisciplinary Sciences, Shahid Rajaei Teacher Training University (SRTTU), 16785-136 Tehran, Iran

² Department of Mechanical Engineering, Jasb Branch, Islamic Azad University, Markazi Province, 37941 Delijan, Iran

³ Solids Design Department, Faculty of Mechanical Engineering, Shahid Rajaei Teacher Training University (SRTTU), 16785-136 Tehran, Iran

Graphic abstract



Keywords Composite · Magnesium alloy · Al₂O₃ · Wear · Hot extrusion · Stir casting

1 Introduction

Having an approximate density of 1.74 g/cm³, magnesium is the lightest structural metal. The high strength-to-weight ratio of magnesium alloys results in lower weight in engineering designs and making them increasingly popular for different industries such as aerospace, military, electronics, automotive, appliances, and sports applications [1]. However, the use of magnesium alloys is limited due to their low mechanical properties, such as strength, toughness, elastic modulus, wear resistance, fatigue resistance,

and creep resistance at high temperatures [2]. To overcome the limitations, the addition of reinforcements significantly improves the mechanical properties and increases the range of magnesium-based composites applications [3].

Stir casting is preferred to other producing techniques for fabricating composite materials due to its simplicity, compatibility, the ability to produce complex shapes, low cost, and high production rate [4–6]. High porosity, inclusions, hot cracks, non-uniform distribution of the reinforcement phase, and other defects in composites produced by stir casting during the solidifying process cause a strong need for

a post deformation process [7]. Such a process is used to decrease porosity and redistribution of the reinforcement phase, and eliminate casting defects [8]. Among the post deformation processes, hot extrusion [9] is believed as a very suitable technique to provide well fragmented and homogeneously distributed intermetallic particles microstructure with fine grain in materials, including metal–matrix composites, in which the successful deformation is hardly achieved [10]. Grain refinement takes place by dynamic recrystallization (DRX) during processing, and it has been reported that the starting temperature for DRX to occur in Mg alloys is 150–175 °C [11]. In fact, once the temperature is high enough, twinning and basal slip deformation mechanisms mostly change to expand the original grain boundaries as well as prismatic and pyramidal slips.

The selection of reinforcement in magnesium–matrix composites depends generally on its price, availability, and compatibility with the base magnesium. Among ceramics, as the common reinforcement materials, Al₂O₃ is a very good reinforcement candidate due to its high strength, hardness, and wear resistance, high melting point and thermal stability, availability, low cost, and chemical neutrality [12]. In recent years, numerous studies were conducted on various hard particle–reinforced magnesium–matrix composites. Al₂O₃ has been shown to form some phases in magnesium melt, and it leads to modification of the interface and adhesion between oxide itself and the melt [13]. However, regarding magnesium–matrix composites, the base materials are limited to a few; mostly include conventional alloys such as AZ31 [14, 15], AZ91 [8, 16], or pure magnesium [17, 18]. Such alloys, which contain aluminum, have low ductility, poor mechanical properties at high temperatures, and low creep resistance, mainly due to the presence of the Mg₁₇Al₁₂ phase [19, 20]. Therefore, it is necessary to develop magnesium alloy-based composites having superior properties.

Studies on tribological properties of different magnesium alloys show that secondary phases that are stable at high temperatures improve wear resistance [21, 22]. The wear test conducted on extruded Mg–Zn–Y alloy shows that the wear rate increases because of grain refining effect, which has been attributed to slip through grain boundaries [23]. Recently, the triple system of Mg–Zn–Ca caught a lot of attention [24–26], but most of the studies have focused

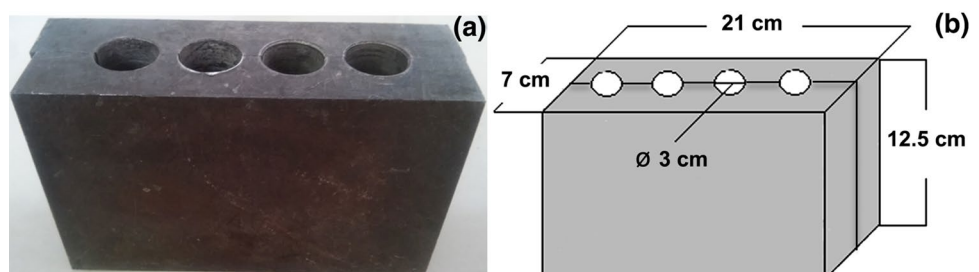
on non-reinforced alloys. In addition, few studies have shown that Mg–Zn–Ca/SiC_p composite possesses adequate mechanical properties in the room and high temperatures [27]. However, it is worth noting that only tensile properties have been studied. Moreover, the reinforcement material was SiC particles. To the best of our knowledge, the wear behavior of Mg–Zn–Ca composite reinforced with Al₂O₃ and undergone hot working, such as hot extrusion, has not been studied, and despite the predicted behavior, investigating the wear behavior of such composite seems to be necessary. Therefore, in this work, the microstructure, hardness and wear behavior are studied for Mg–6Zn–1Ca-based composite having three different volume percentages of Al₂O₃ particles, produced by stir casting process followed by hot extrusion at 300 °C, 350 °C and 400 °C.

2 Experimental

2.1 Materials and sample preparation

In order to produce the required composites, Mg–6Zn–1Ca alloy and Al₂O₃ particles, with an average diameter of approximately 5 μm, were used as the base and reinforcing materials, respectively. Stir casting followed by hot extrusion was used to prepare the composites for the study. In other words, two types of samples, cast and extruded, were fabricated for the investigation. Melting, alloying, and composite making processes were performed in a heat-resistant steel crucible in an electrical resistance furnace (Azar furnaces, VM10L1200) at 800 °C. While Al₂O₃ reinforcing particles were added to the molten metal, it was stirred by a graphite blade for 5 min at the speed of 400 rpm. In order to provide better distribution of particles and avoid dead zones in the molten metal, the blade was moved in both vertical and horizontal directions. Afterward, the molten composite was poured into a 250 °C preheated steel mold shown in Fig. 1 to produce cast composites with nominal percentages of 0% (no reinforcement), 2.25%, 4.5% and 6.75% Al₂O₃ in a cylindrical shape (billet) with a diameter of 3 cm and height of 12.5 cm. All processes, including melting, alloying, composite making and pouring, were controlled throughout the process by pure argon gas at 1 l/min pressure rate in order

Fig. 1 Steel mold used for casting; **a** the real picture and **b** a schematic image



to prevent the melt oxidation. The billets were machined to cylindrical pieces of approximately 3 cm in diameter and 4.5 cm in height for the next hot extrusion process. A cylindrical electrical resistance furnace was used to enclose the billets as well as the ram, container and die to provide the desirable required temperatures of 300 °C, 350 °C and 400 °C, for the extrusion process. Heating was sustained for an hour, before the process, to ensure a stable temperature for the billet and setup. Then, a hydraulic servo press with a capacity of 1000 kN and a constant ram speed of 1 mm/s was used to apply the required pressure to fabricate the extruded samples at the extrusion rate of 10:1. The produced extruded composites were cooled down to room temperature in still air.

2.2 Microstructure study and phase analysis

In order to carry out microstructural study, the cast and extruded samples were prepared according to the ASTM E3-11 standard and ground with SiC papers up to a final of 2500 grit, then polished using diamond paste with the size of 6 µm, and finally etched with 4% Naital solution for 20 s according to the ASTM E407-7 e1 to reveal the microstructure and grain boundaries. Optical microscope (OM, Aristomet), scanning electron microscope (SEM, SEM, Vega3 Tescan) equipped with energy-dispersive X-ray spectroscopy (EDS), and Ultima IV X-ray diffractometer (XRD) with Cu- α radiation were used to study the microstructures. To analyze the resulting XRD patterns, X'Pert HighScore Plus software (Version b2.2) was used.

2.3 Hardness and pin-on-disk wear tests

A Brinell hardness testing machine (Ernst, NR3D) was used to measure the hardness of the cast and extruded composites according to the ASTM E10-18 standard, by applying a load of 62.5 kgf and ball size of 2.5 mm for 15 s. The specimens were prepared as per the standard procedure. An average of four hardness measurements read from four different locations each was reported. In order to determine the wear resistance, the pin-on-disk method was used under dry sliding conditions according to the ASTM G99-17 standard. In this method, samples of the cast alloy, as well as the cast and extruded composites with the diameter of 6 mm and height of 15 mm, were utilized as the pins and ASTM 52,100 bearing steel with the diameter of 30 mm having the hardness of 64 HRC was chosen as the disk. After grinding manually up to 2500 grit SiC papers, polishing with 1.0 and 0.05 µm alumina powder slurry, cleaning ultrasonically, and drying, the samples were weighed with an accuracy of 0.0001 g before and after the wear test. In order to provide reliable results, the wear test was repeated thrice for each sample and the average values are taken to determine the wear rate. The

wear test conditions are given in Table 1. The surface of the samples was studied by SEM after the wear test to reveal the wear mechanism taken place.

3 Results and discussion

3.1 Microstructures characterizations

The SEM micrograph of the cast composite, having 2.25 vol.% Al₂O₃, is shown in Fig. 2a. In addition, the EDS spectra of the denoted points, A, B, and C, in the microstructure are shown in Fig. 2b-d. As can be seen, the micrograph is composed of grains (A) and continuous (B) as well as spherical (C) deposits formed on the grains boundary and matrices, respectively, and some particles of Al₂O₃. According to the EDS analysis results, it can be inferred that the grains are solid solution of zinc in magnesium, known as α -Mg (Fig. 2b), and the deposits are identical intermetallic composed of three elements of Mg, Zn, and Ca (Fig. 2c and d). More accurately, the X-ray diffraction pattern (Fig. 3) reveals that the microstructure of the composite matrix consists of only two phases of α -Mg and hexagonal ternary Ca₂Mg₆Zn₃. It should be noted that in ternary systems of Mg–Zn–Ca, apart from α -Mg, if the atomic ratio of Zn/Ca is larger than 1.2, then only Ca₂Mg₆Zn₃ is deposited; but, if the ratio is lower than 1.5, then in addition to Ca₂Mg₆Zn₃, another intermetallic, Mg₂Ca, is formed [28, 29]. In other words, in Zn/Ca ratios less than 1.5, having excessive Ca compared to what is required to form Ca₂Mg₆Zn₃, the condition for the formation of another intermetallic Mg₂Ca is provided. In the present alloy (matrix of the composite), as the Zn/Ca ratio is around 3.7, only two phases of α -Mg and Ca₂Mg₆Zn₃ are present in the microstructure, and the results are in agreement with those reported by other researchers [30, 31].

The SEM micrographs of the cast composites are shown in Fig. 4. As can be observed, increasing the volume percentage of Al₂O₃ particles leads to a more uniform distribution of the particles in the microstructure. It can also be seen that the microstructure of the base alloy becomes finer and the grains are smaller.

Table 1 Pin-on-disk test conditions

Parameter	Unit	Value
Load	N	3, 9, 15, and 21
Pin movement diameter on samples	mm	13
Pin rotation speed on samples	rpm	600 (equivalent to about 0.4 m/s)
Test duration for each sample	min	43
Wear length for each sample	m	1054

Fig. 2 **a** An SEM image of the microstructure of cast composite containing 25 vol.% Al₂O₃; and **b-c**) EDS spectra of different constituents denoted with points A, B, and C, respectively

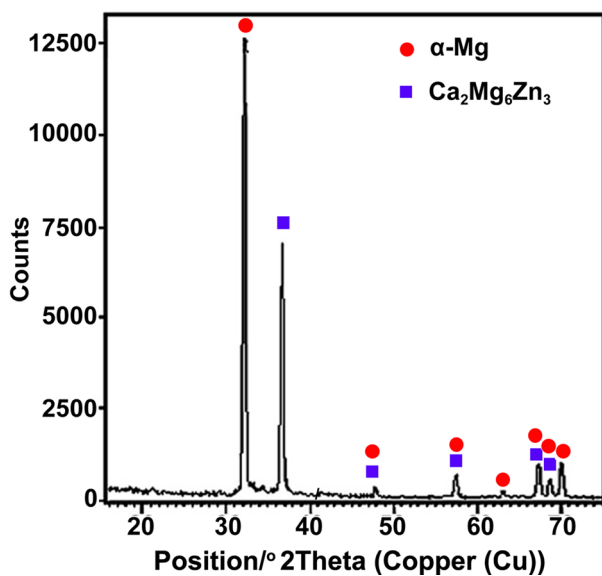
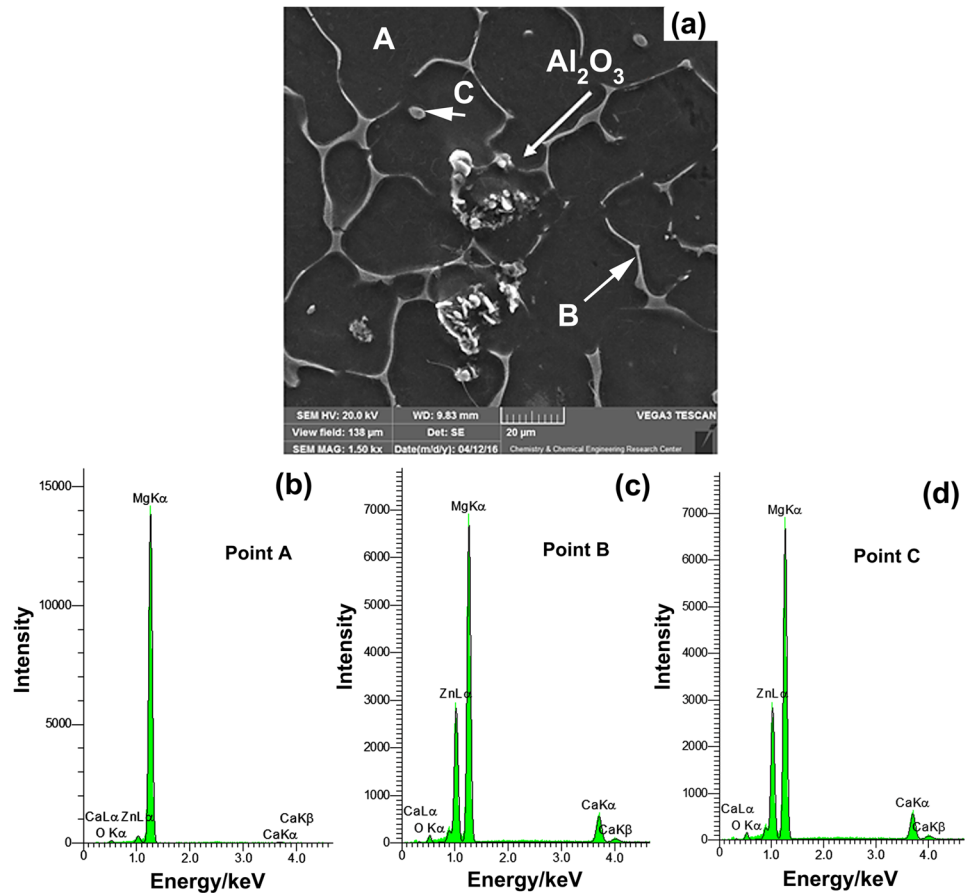


Fig. 3 XRD pattern of the composite matrix

This is more evident when the microstructure of non-reinforced alloy (Fig. 4a) is compared with that of the composite having 6.75 vol.% of Al₂O₃ particles (Fig. 4b). In general,

the addition of reinforcing particles to magnesium alloys decreases the grain size. This effect is more pronounced in the grains located at the Al₂O₃-cluster zones. On one hand, grain refining happens due to the heterogeneous nucleation of magnesium grains on the reinforcing particles, as especially Al₂O₃ has a similar structure to that of magnesium, hexagonal; on the other hand, external particles prohibit grain growth during the solidification process. Moreover, as can be seen from Fig. 4b–d, there are Al₂O₃-cluster and Al₂O₃-free regions in the microstructures that are common in stir cast composites, which can be attributed to the push effect of solidification front [32]. The latter needs post mechanical working to improve the microstructure. Also, the presence of porosity between the grains and the agglomeration of reinforcement particles is other evidence of the cast composite microstructure.

Figure 5 represents typical images of the porosity and agglomeration in the cast composite containing 2.25 vol.% Al₂O₃. Such defects have been reported by other researchers as well [33]. Optical non-etched images of microstructures of the cast and 4.5 vol.% Al₂O₃ containing Mg-6Zn-1Ca alloy extruded at 350 °C and 400 °C are shown in Fig. 6. The prominent feature of the images is the significant stretched and more uniform distribution of Al₂O₃ particles aligned the

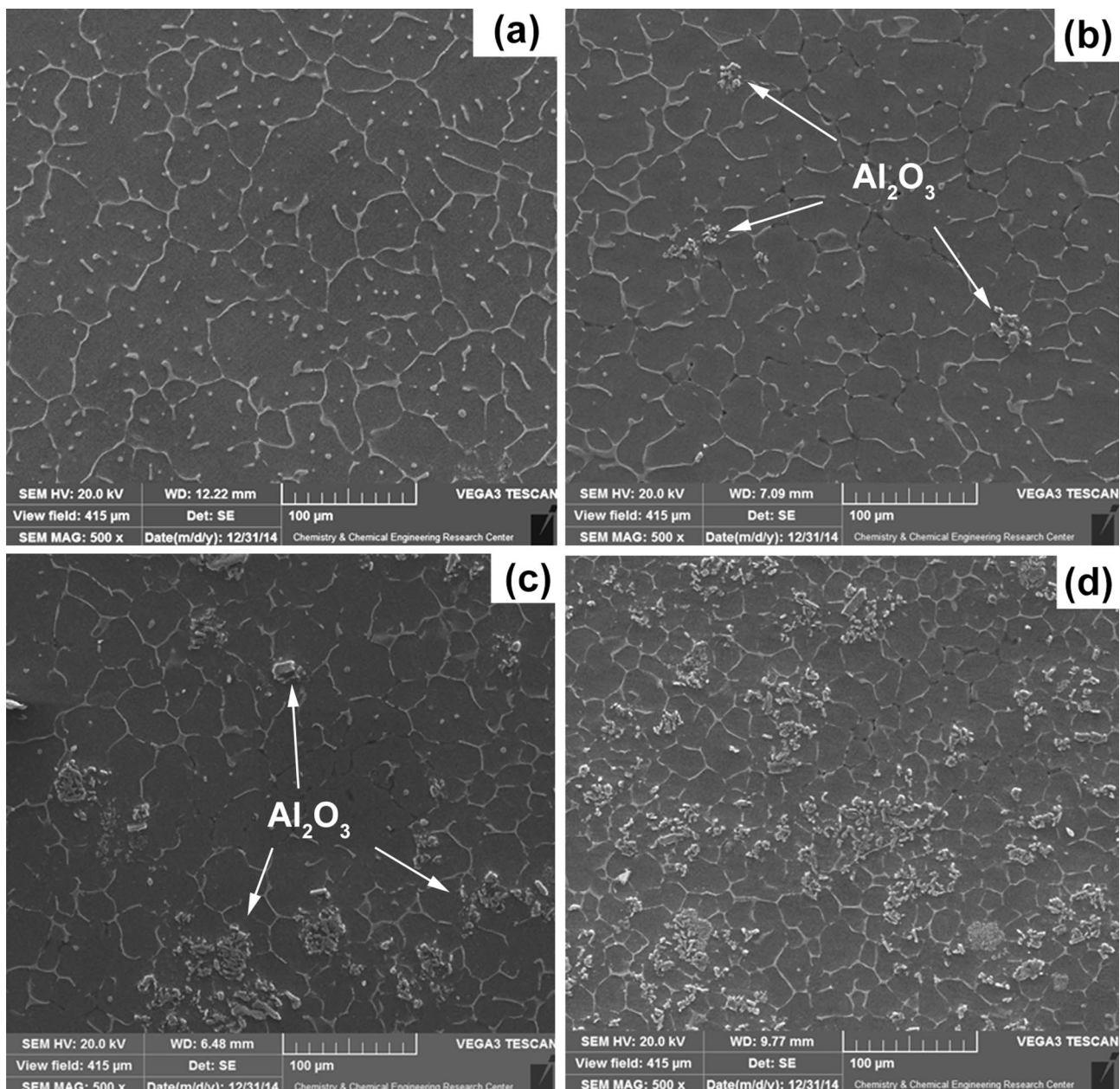


Fig. 4 SEM micrographs of the cast composites containing **a** zero, **b** 2.25, **c** 4.5, and **d** 6.75 vol.% Al_2O_3

extrusion direction. Besides, no porosity can be seen in the microstructure of the extruded composites. In other words, the softer matrix of the composite plastically deforms, but the brittle Al_2O_3 particles resist deforming during the hot extrusion, causing piling-up of shear stress at the particles and breaking them up, resulting in a more close distribution of the particles in the matrix [31].

Figure 7 shows SEM micrographs of the 4.5 vol.% Al_2O_3 bearing composite after extrusions at 350 °C and 400 °C. It can also be seen that extrusion at 400 °C leads to finer particles in the microstructure when compared

to that extruded at 350 °C, which can be ascribed to the easier flow of the materials at higher temperatures. In other words, as mentioned earlier, by increasing extrusion temperature, the easier flow of the alloy causes more deformation, while, due to the brittle nature, Al_2O_3 particles and intermetallic $\text{Ca}_2\text{Mg}_6\text{Zn}_3$ are broken up to provide finer particles. Similar observations are reported by other researchers such as WANG et al. [27] for Mg–Zn–Ca/SiC_p composite. They also reported the possible presence of nanosize particles after extrusion.

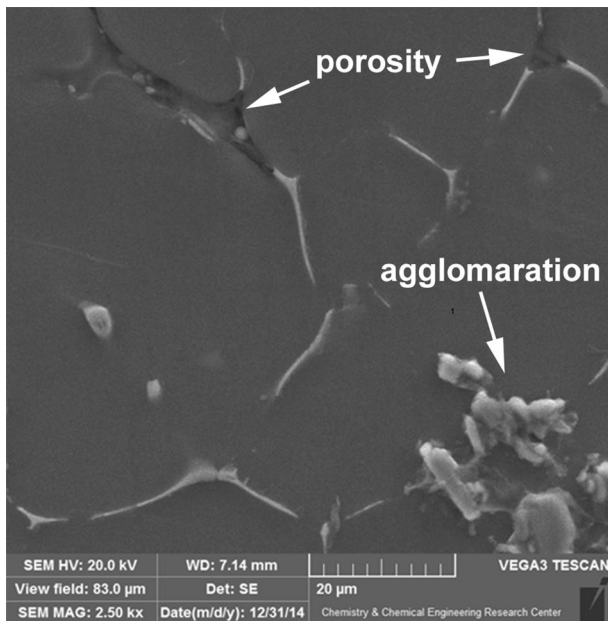


Fig. 5 An SEM image of the microstructure of cast composite containing 2.25 vol.% Al₂O₃ showing porosity and agglomeration

3.2 Hardness

Figure 8 depicts the results of Brinell hardness measurements performed on the cast and extruded composites. It clearly shows that hardness values increase linearly in the composites when the volume percentage of Al₂O₃ particles rises up. Increasing Al₂O₃ particle content results in enhanced resistance of the composites against indentation, which, in turn raises the composite hardness. The curves also show that increasing Al₂O₃ reinforcing particle content from 2.25 vol.% to 6.75 vol.% improves the composite hardness as much as 24%, although 2.25 vol.% Al₂O₃ bearing composite shows a slight increase (3.3%) in hardness, suggesting that the addition of 2.25 vol.% Al₂O₃ particle is not enough for desired improvement in the hardness. In the extruded composites, in addition to the resulting strain and work hardening caused by the extrusion process, the reduced grain size, due to the dynamic recrystallization, more homogeneous distribution of the Al₂O₃ particles in the matrix, and stronger bonding between the particles and matrix, hardness of the composites improves significantly compared to the cast one. The hardness increase for the composites extruded at 350 °C and 400 °C, having different volume percentages of Al₂O₃ particles, is approximately 31–36

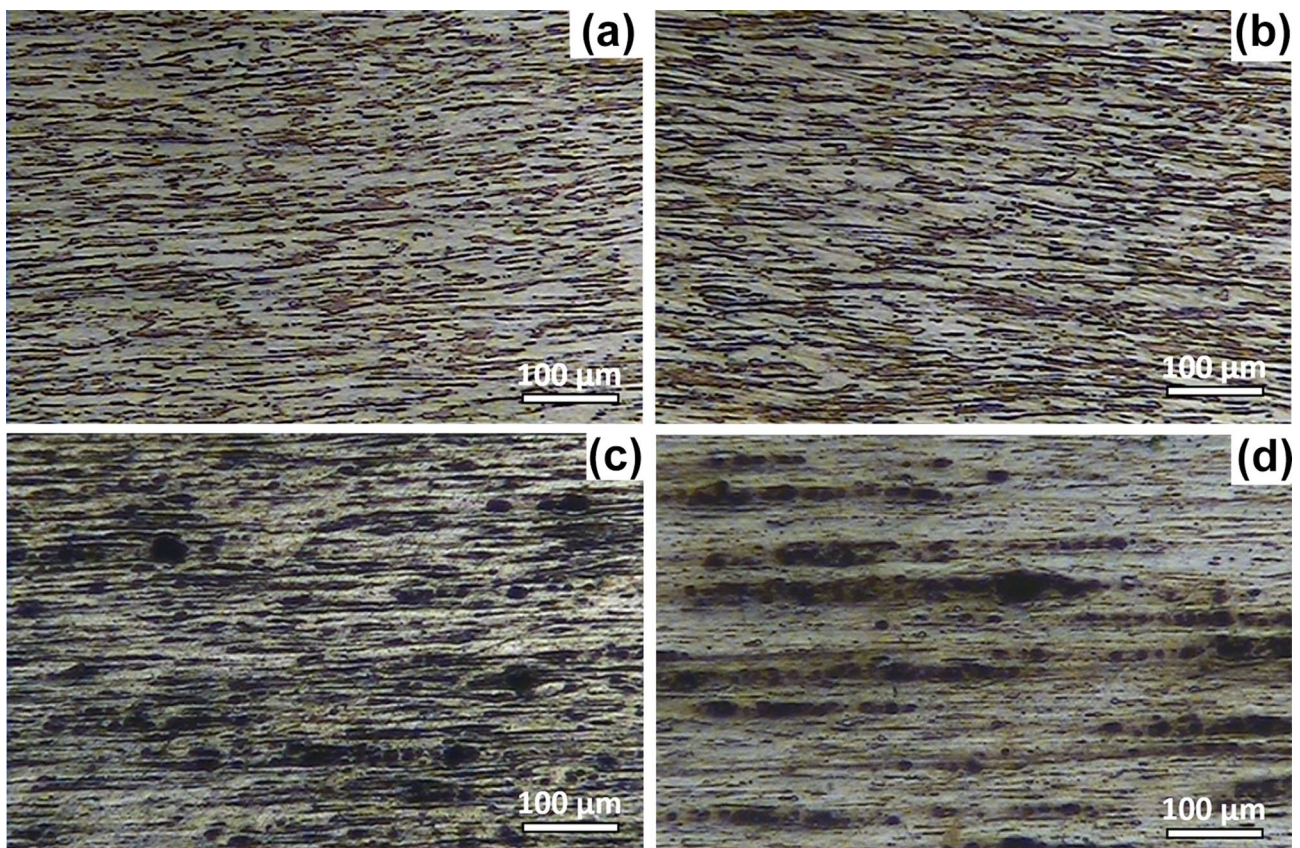


Fig. 6 Optical non-etched microstructures images (normal to extrusion direction) of (a and b) Mg-6Zn-1Ca alloy and (c and d) Mg-6Zn-1Ca/4.5 vol.% Al₂O₃ composite after extrusion at 350 °C and 400 °C, respectively

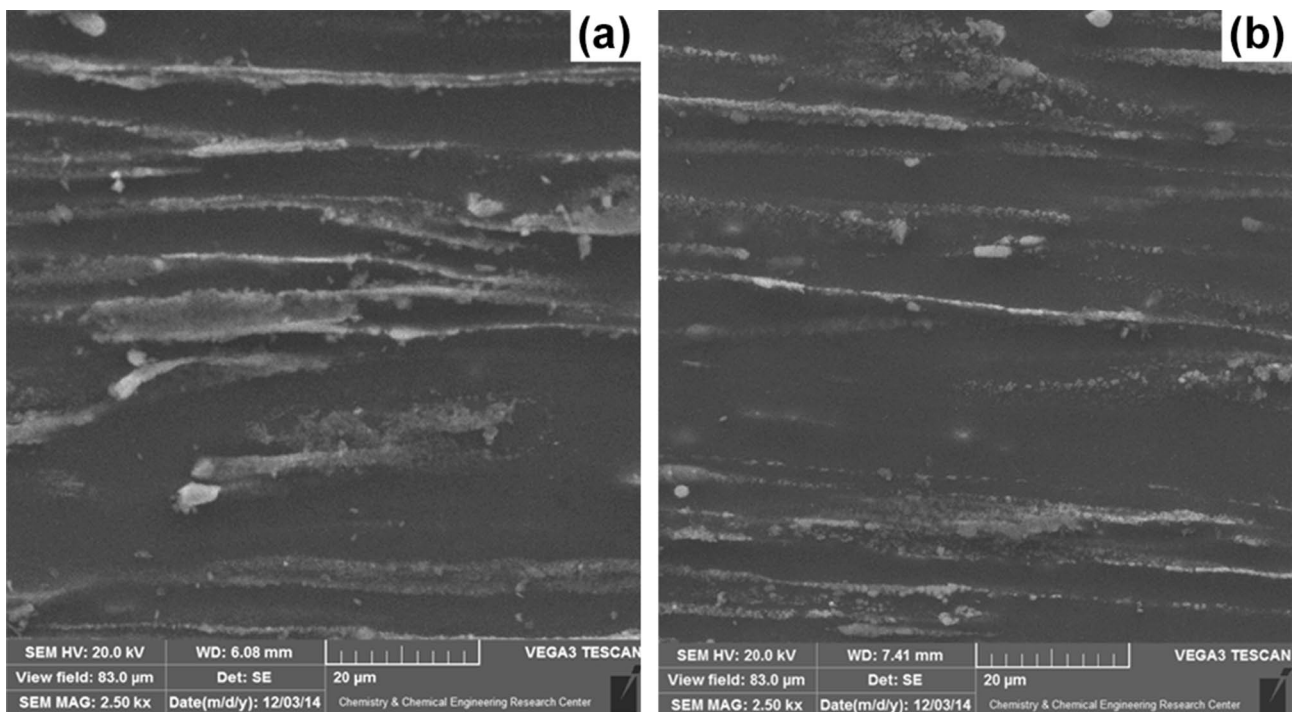


Fig. 7 SEM micrographs of Mg-6Zn-1Ca/4.5 vol.% Al₂O₃ composite after extrusion at **a** 350 °C and **b** 400 °C

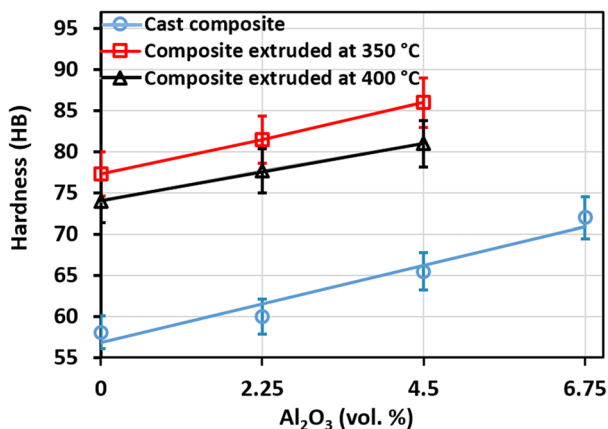


Fig. 8 Hardness values of cast and extruded composites as a function of volume percentage of Al₂O₃ particles

and 24–30%, respectively. The lower improvement (5–6%) in hardness (H) of the composites extruded at the higher temperature (400 °C) can be attributed to the slight increase in the size of recrystallized grains, according to the Hall–Petch equation (Eq. 1) [34]:

$$H = H_o + \frac{K}{\sqrt{D}} \quad (1)$$

In this equation, H_o is the hardness of annealed material, D is the grain size, and K is a constant. It should be noted that the available hydraulic servo press with the capacity of 1000 kN was unable to properly extrude the 6.75 vol.% Al₂O₃ composite due to the very high strength of the composite.

3.3 Wear

Figure 9 shows the wear rate of the cast alloy and composites as a function of the normal applied load. It shows an almost linear increase in wear rate when the applied load rises, as other researchers reported as well [35]. On the other hand, as can be seen, the addition of 2.25 vol.% Al₂O₃ reinforcing particles causes the wear rate of the cast alloy to decrease due to the three reasons of (1) higher hardness of the reinforcing particles, (2) lower contact area between the composite matrix and counterface steel, and (3) higher resistance of matrix to plastic deformation [36], leading to higher hardness material (Fig. 8). The reduction in wear rate is calculated as 35.1% and 10.1% for the samples undergone 3 and 21 N, respectively. This is more pronounced in the composite containing 4.5 vol.% Al₂O₃, in which increasing the amount of Al₂O₃ particles decreases the wear rate of the composite for 92.8% and 17.6% when it is subjected to 3 and 21 N, respectively. Similar results were reported by SHARMA et al. [37] while studying wear properties of magnesium matrix composites reinforced with feldspar.

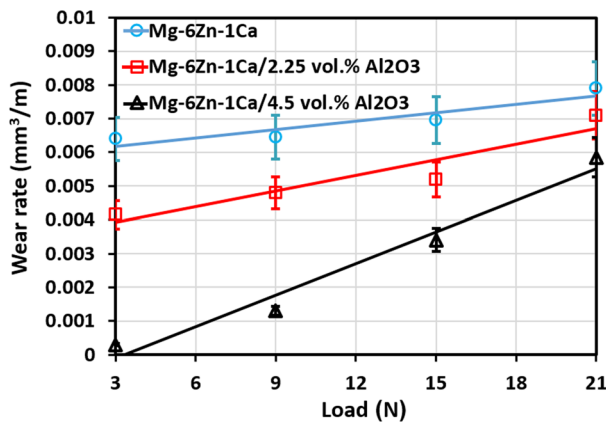


Fig. 9 Effect of Al₂O₃ content on wear rate of cast alloy and composites

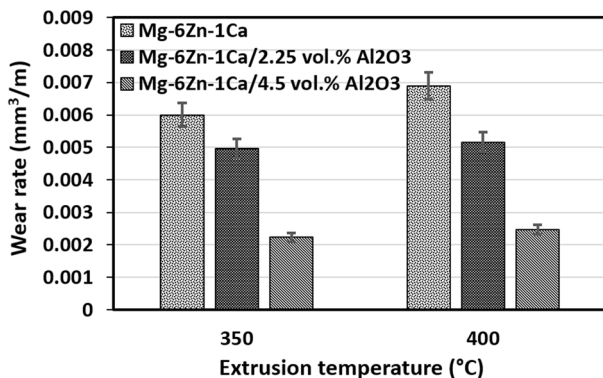


Fig. 10 Wear rate values of the extruded alloy and composites as a function of extrusion temperature (Load: 21 N)

In the wear behavior investigation of the extruded alloy and composites, as can be seen in Fig. 10, not only the extrusion process enhances the wear resistance of the Mg-6Zn-1Ca alloy, but also almost similar improvements are obtained for the extruded composites containing 2.25 vol.% and 4.5 vol.% Al₂O₃. The improvements are calculated as 24% and 12.6% for the alloy extruded at 350 °C and 400 °C, respectively, compared to the cast one. In contrast, the improvement is calculated as 29.6% and 28.2%, and 64.2% and 59.3% for the 2.25 vol.% and 4.5 vol.% Al₂O₃ bearing composites extruded at 350 °C and 400 °C, respectively. The improvement in the wear rate of the extruded alloy and composites is attributed to the reasons of high hardness of Al₂O₃, higher uniformity of the Al₂O₃ particles in the matrix of composite, and the improvement in the interface between the particles and matrix [36]. In addition, the main reason for the increased wear resistance of the extruded samples can be explained by the Archard equation (Eq. 2):

$$V = \frac{LkW}{H} \quad (2)$$

where V is the volumetric wear volume (mm³), L is the sliding distance (m), W is the normal applied load (N), k is the wear coefficient, and H is the hardness of the sample (kN/mm²). According to Eq. (2), the wear rate (V/L) is proportional to the applied load (assuming the average sizes of the contact area and the abrasion particles are constant), and it is independent of the contact area shape. Although this equation predicts that the wear resistance of the materials depends on their hardness, the relationship between the wear rate and the microstructure of the materials has not been considered. In other words, considering the microstructure of the experimented composites, the relationship between the hardness and wear resistance of the composites is complicated, although wear rate of the composites is determined by the wear rate of the harder phase in microstructure, meaning Al₂O₃ particles. On the other hand, considering the extrusion temperature, it can be inferred that the increased temperature results in deterioration of the wear resistance. In fact, even though conducting extrusion process at higher temperature leads to a more uniform distribution of the Al₂O₃ particles and improves wear properties; however, due to the decreased hardness caused by reduced work hardening, as well as the grain growth, the wear rate of the extruded alloy and composites experiences a slight increment.

In order to study the morphology of the surfaces after wear test and identifying the wear mechanism, the surfaces were studied using SEM. Figure 11 represents typical SEM images from the surface of the cast and Mg-6Zn-1Ca/2.25 vol.% Al₂O₃ composites extruded at both 350 °C and 400 °C after wear test. From the images, it can easily be seen that the surfaces of the extruded composites are smoother and have lesser deformed areas compared to that of the cast composite. The images also display that the surfaces include continuous scratches parallel to the wear direction, plastic deformation, and delamination. In other words, it can be stated that there are three wear mechanisms of delamination, abrasion, and plastic deformation or adhesion. Almost similar mechanisms were reported by MEENASHISUNDARAMI and GUPTA [39]. It should be noted that materials with the microstructures containing secondary hard phases, like the present experimented composites, Al₂O₃ particles break into smaller particles due to the plastic deformation during the wear test. The formation of voids around the hard particles during deformation of the composite matrix originated from the wear test, as well as the crushed particles. It nucleates cracks followed by crack growth and results in cracks propagation, which causes delamination defect on the surface of the composite surfaces [40]. In addition, the crushed Al₂O₃ particles, trapped between surfaces of the sample and pin, act as abrasive particles to provide abrasive

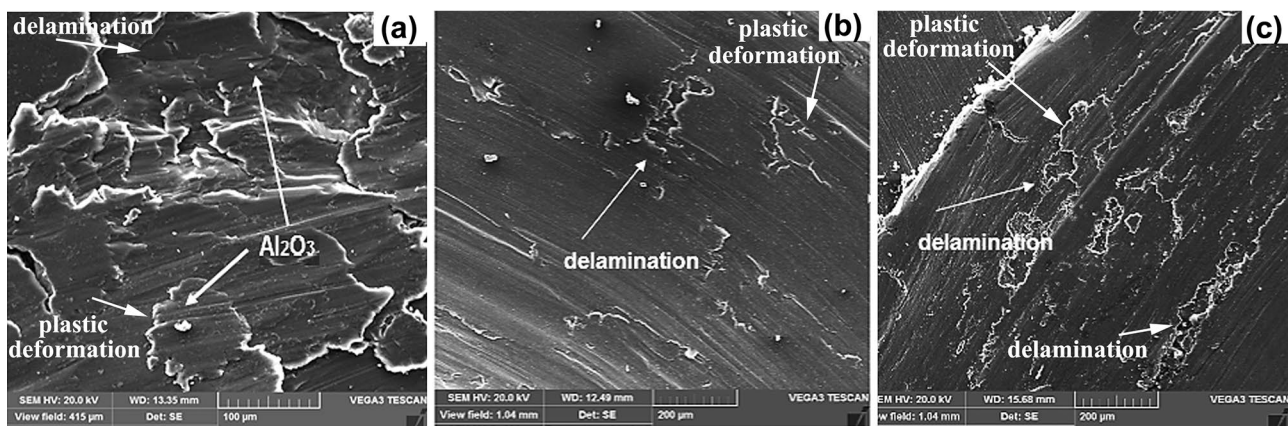


Fig. 11 SEM images from the surface of Mg-6Zn-1Ca/2.25 vol.% Al_2O_3 composite after wear test; **a** cast sample, **b** sample extruded at 350 °C, and **c** sample extruded at 400 °C

wear. Moreover, because of lower hardness, the matrix of the composites shows less wear resistance, and it is more affected by the adhesive wear mechanism. Figure 11a shows the SEM image of the cast composite surface after wear test. As marked on the image, the delamination and plastic deformation wear mechanisms along with scratches caused by the abrasive wear mechanism are very clear. In comparison, Fig. 11b and c designates that the signs of delamination and plastic deformation wear mechanisms are much less prominent on the surface of the extruded samples. The SEM images shown in Fig. 11b and c also indicate that the wear defects are more visible on the surface of the composite extruded at 400 °C compared to that extruded at 350 °C. In other words, the composites extruded at 400 °C show lower resistance to wear and it is attributed to the hardness diminishes as discussed in Sect. 3.2. In general, the presence of scratches caused by wear through pin movement as well as the crushed and separated Al_2O_3 particles in the interface between disc and pin shows that abrasive wear is the dominant wear mechanism taken place on the surface of the composite extruded at 350 °C. In contrast, all three wear mechanisms of abrasion, delamination, and adhesion involve on the worn surface of both the cast composite and the composite extruded at 400 °C, although delamination and adhesive wear mechanisms are more pronounced on surface of the cast composite.

4 Conclusions

In this study, Mg-6Zn-1Ca matrix composites, containing 2.25, 4.5, and 6.75 vol.% Al_2O_3 , were produced by stir casting, then subjected to extrusion process at three temperatures of 300, 350 and 400 °C, and finally, their wear behavior was investigated. The following conclusions can be stated:

1. Microstructure of the composite matrix is composed of α -Mg solid solution, in which intermetallic $\text{Ca}_2\text{Mg}_6\text{Zn}_3$ mostly formed on the grain boundaries. The addition of reinforcing Al_2O_3 particles results in the reduction of grain size of the matrix. The apparent stretching of the microstructure and finer Al_2O_3 particles of the composite extruded at higher temperature are of the notable features of the microstructure of the extruded composites.
2. Increasing Al_2O_3 content increases the hardness and decreases the wear rate in both cast and extruded composites. However, the elevation of the extrusion temperature increases the wear rate slightly due to the decreased work hardening effect and grain growth. As a result, the composites extruded at 350 °C show the least wear rate among the experimented alloy and composites.
3. Although the extrusion process results in an increased hardness of the cast composites, increasing the extrusion temperature from 350 to 400 °C decreases the hardness slightly due to a small increase in the recrystallized grains size.
4. Abrasion is the dominant wear mechanism in the composites extruded at 350 °C, while in both the cast composite and these extruded at the higher temperature, abrasion, delamination and adhesion are the realized wear mechanisms, although delamination and adhesion are dominant wear mechanisms in cast composites.

Acknowledgements The authors are very thankful to the Shahid Rajaei Teacher Training University for supporting this research.

Declaration

Conflict of interest The authors declare no financial or commercial conflict of interest.

References

1. A. Ghanbari, H. Jafari, F. Ashenai Ghasemi, *Met. Mater. Int.* **26**, 395 (2020).
2. D. Sameer Kumar, K. N. S. Suman, P. Poddar, *Can. Metall. Quart.* **57**, 455 (2018).
3. X. Zhou, L. Li, D. Wen, X. Liu, C. Wu, *Trans. Nonferr. Metal. Soc. China* **28**, 440 (2018).
4. N. Anand, K.K. Ramachandran, D. Bijulal, *Mater. Today Proc.* (2020).
5. E.N. Galashov, A.A. Yusuf, E.M. Mandrik, V.V. Atuchin, *Int. J. Adv. Manuf. Technol.* **86**, 475 (2016).
6. K.V. Dorozhkin, G.E. Dunaevsky, S.Y. Sarkisov, V.I. Suslyaeov, O.P. Tolbanov, V.A. Zhuravlev, Y.S. Sarkisov, V.L. Kuznetsov, S.I. Moseenkov, N.V. Semikolenova, V.A. Zakharov, V.V. Atuchin, *Mater. Res. Express.* **4**, 106201 (2017).
7. X. Wang, C. Chen, M. Zhang, *App. Phys. A.* **126**, 714 (2020).
8. H. Chang, X. Hu, X. Wang, J. Du, L. Tong, *J. Mater. Res.* **34**, 335 (2019).
9. F. Khorasani, M. Emamy, M. Malekan, H. Mirzadeh, B. Pourbahari, T. Krajnák, P. Minárik, *Mater. Charact.* **147**, 155 (2019).
10. Y.W. Wu, K. Wu, K.K. Deng, K.B. Nie, X.J. Wang, X.S. Hu, M.Y. Zheng, *Mater. Sci. Eng. A.* **527**, 6816 (2010).
11. M. Shiri, H. Jafari, *JOM* **71**, 4705 (2019).
12. T. Thirugnanasambandham, J. Chandradass, P. Baskara Sethupathi, M. Leenus Jesu Martin, *Mater. Today Proc.* **14**, 211 (2019).
13. E. Ghasali, A. Bordbar-Khiabani, M. Alizadeh, M. Mozafari, M. Niazmand, H. Kazemzadeh, T. Ebadzadeh, *Mater. Chem. Phys.* **225**, 331 (2019).
14. R. V. P. Kaviti, D. Jeyasimman, G. Parande, M. Gupta, R. Narayanasamy, P. G. Koppad, *Mater. Res. Express.* **6**, 126505 (2019).
15. M. Azizieh, A. Norouzi Larki, M. Tahmasebi, M. Bavi, E. Alizadeh, H.S. Kim, *J. Mater. Eng. Perform.* **27**, 2010 (2018).
16. H. Liu, N. Lu, X. Wang, *Met. Mater. Int.* (2020).
17. J. Zhu, J. Qi, D. Guan, L. Ma, R. Dwyer-Joyce, *Tribol. Int.* **146**, 106253 (2020).
18. K. Balamurugan, M. Uthayakumar, S. Thirumalai Kumaran, G.S. Samy, U.T.S. Pillai, *Defence Technol.* **15**, 557 (2019).
19. G. Levi, S. Avraham, A. Zilberov, M. Bamberger, *Acta Mater.* **54**, 523 (2006).
20. M. Bamberger, G. Levi, J.B. Vander Sande, *Metall. Mater. Trans. A.* **37A**, 481 (2006).
21. J. An, R. Li, Y. Lu, C. Chen, Y. Xu, X. Chen, L.M. Wang, *Wear* **265**, 97 (2008).
22. A. Barylski, M. Kupka, K. Aniolek, J. Rak, *Vacuum* **139**, 77 (2017).
23. H. Somekawa, A. Shimoda, T. Hirayama, T. Matsuoka, T. Mukai, *Mater. Trans.* **55**, 216 (2014).
24. H. Li, S. Qin, Y. Ma, J. Wang, Y. Liu, J. Zhang, *Int. J. Min. Met. Mater.* **25**, 800 (2018).
25. A.S. Abdel-Gawad, M.A. Shoeib, *Surf. Interf.* **14**, 108 (2019).
26. R. Rahmany-Gorji, A. Alizadeh, H. Jafari, *Mater. Sci. Eng. A.* **674**, 413 (2016).
27. X.J. Wang, K.B. Nie, X.S. Hu, Y.Q. Wang, X.J. Sa, K. Wu, *J. Alloy. Compd.* **532**, 78 (2012).
28. Y. Ma, C. Yang, Y. Liu, F. Yuan, S. Liang, H. Li, J. Zhang, *Int. J. Min. Metall. Mater.* **26**, 1274 (2019).
29. J. Yang, J. Peng, M. Li, E. A. Nyberg, F. Pan, *Acta Metall. Sinica (Engl. Lett.)* **30**, 53 (2017).
30. K. Nie, Z. Zhu, P. Munroe, K. Deng, J. Han, *J. Mater. Sci.* **55**, 3588 (2020).
31. F. Doost Mohammadi, H. Jafari, *Trans. Nonferrous Met. Soc. China.* **28**, 2199 (2018).
32. X. Wang, X. Hu, K. Nie, K. Wu, M. Zheng, *Trans. Nonferrous Met. Soc. China.* **22**, 1912 (2012).
33. B. Ram, D.D. Drivadi, N. Bala, *Mater. Res. Express.* **6**, 066555 (2019).
34. S. S. Razavi Tousi, R. Yazdani Rad, E. Salahi, I. Mobasherpour, M. Razavi, *Powder Technol.* **192**, 346 (2009).
35. S. Ataya, N. Alsaleh, M. E. Soleman, *Acta Metall. Sinica (Engl. Lett.)* **32**, 31 (2019).
36. F. Aydin, Y. Sun, *Can. Metall. Quart.* **57**, 455 (2018).
37. S.C. Sharma, B. Anand, M. Krishna, *Wear* **241**, 33 (2000).
38. B. Mao, X. Zhang, P. L. Menezes, Y. Liao, *Materialia.* **8**, 100444 (2019).
39. G.K. Meenashisundarami, M. Gupta, *JOM.* **68**, 1890 (2016).
40. N. Soltani, H. Jafari Nodooshan, A. Bahrami, M. I. Pech-Canul, W. Liu, G. Wu, *Mater. Des.* **53**, 774 (2014).

Publisher's Note Springer Nature remains neutral with regard to jurisdictional claims in published maps and institutional affiliations.